Wavelet-based crack identification of bridge beam from operational deflection time history

X.Q. Zhu, S.S. Law [*]

Civil and Structural Engineering Department, Hong Kong Polytechnic University, Hunghom, Kowloon, Hong Kong, People's Republic of China

Abstract

A new method for crack identification of bridge beam structures under a moving load based on wavelet analysis is presented. Crack is modeled through rotational springs whose compliance is evaluated using linear elastic fracture mechanics. Dynamic behavior of the cracked beam subject to moving load is analyzed using mode superposition. The response obtained at a single measuring point is analyzed using continuous wavelet transform and the location of the cracks is estimated. The locations of the cracks are determined from the sudden changes in the spatial variation of the transform responses. To estimate the relative depth of the cracks, a damage factor is established which relates the size of the cracks to the coefficients of the wavelet transform. The proposed method is validated by both simulation and experiment. Locations of multiple damages can be located accurately, and the results are not sensitive to measurement noise, speed and magnitude of moving load, measuring location, etc.
© 2005 Elsevier Ltd. All rights reserved.

Keywords: Moving load; Bridge; Dynamics; Wavelet; Damage detection; Inverse problem; Operation deflection shape

1. Introduction

The detection of crack-like defect in mechanical systems and civil engineering structures is a problem that received considerable attention from researchers in the last two decades (Salawu, 1997; Doebling et al., 1998). A crack in a structure introduces local flexibility and changes dynamic characteristics of the structure. There is a large number of nondestructive methods for crack detection that are based on the changes in the dynamic properties of the structure (frequencies, mode shapes, transfer functions,

---

[*] Corresponding author. Tel.: +85227666062; fax: +85223346389.
E-mail address: cesslaw@polyu.edu.hk (S.S. Law).

etc.) caused by the damage. The methods based on natural frequency changes have the principal attraction of using only a reduced set of experimental data that is easily measured and less contaminated by experimental noise. The mode shape inherently is the geometry of the system, and a damage may directly lead to geometric changes of the system. Farrar and Jauregui (1998) presented a comparative study of damage identification algorithms applied to a bridge, and found that standard modal properties such as resonant frequencies and modal shapes are poor damage indicators. Changes in modal properties resulted from changes in environmental conditions can be as significant as the changes in these properties caused by damage (Abdel Wahab and De Roeck, 1997).

Pandey et al. (1991) showed that the curvature of mode shape is more sensitivity to damage than the mode shapes itself. By plotting the difference of modal curvature from the intact and the damage states, a peak at the damaged element indicates the presence of a fault. Hoerst and Ratcliffe (1997) and Ratcliffe and Bagaria (1998) presented a gapped smoothing method, which essentially aimed at extracting certain peaks, which are characteristic of local damages, by processing the curvature mode shape from only the damaged state. However, the curvature changes could be masked by the derivative operations in the presence of noisy data (Chance et al., 1994). Measurement noise significantly affects the success of the processing technique. In most of the methods, the baseline information from the undamaged structure is needed in detecting the damage conditions. How to extract damage signals from the measured dynamic response without using a structural model for reference is a major problem for researchers in dynamics-based damage detection.

In the last decade, wavelet theory has been one of the emerging and fast-evolving mathematical and signal processing tools for vibration analysis. Staszewski (1998) presented a summary of recent advances and applications of wavelet analysis for damage detection. Kijewski and Kareem (2003) studied wavelet transforms for system identification in civil engineering. The main advantage of the continuous wavelet transform is its ability to provide information simultaneously in time and scale with adaptive windows. An application of wavelet theory in the spatial domain crack identification of structures was proposed by Liew and Wang (1998). The wavelet in the spatial domain is calculated based on finite difference solutions of a mathematical representation of the structure in question. The crack location is indicated by a peak in the variations of the wavelets along the length of the beam. Wang and Deng (1999) proposed that the wavelet transform be directly applied to spatially distributed structural response signals, such as surface profile, displacement, strain or acceleration measurements. The continuous wavelet transform of the fundamental mode shape and its Lipschitz exponent was used to detect the damage location and extent in a beam by Hong et al. (2002), Gentile and Messina (2003), Douka et al. (2003) and Chang and Chen (2003). The key point of this method is to check on the spatially distributed response signals that can pick up damage information. A classical measurement system as, for example, an impulse hammer technique is only able to measure mode shapes at a few discrete points of a transversely vibrating beam. Therefore, new sensors or measuring techniques are needed to pick up the perturbations caused by the presence of a crack. Recently, Pai and Young (2001) reported the possibility of measuring displacements on denser grids (a few hundred of points) by using a laser scanning vibrometer.

One of the questions that is attracting significant research attention is related to the use of structural response from operational dynamic loads in a damage detection procedure. For bridges, the operational loads are moving vehicular loads, and the operational deflection shapes are the deflections of the bridge deck subject to moving vehicular loads. Previous studies are mainly on the problem of modal testing and analysis of structures under operational loads. Mazurek and Dewolf (1990) conducted the laboratory studies on simple two-span girders under moving loads with structural deterioration by vibration analysis. Structural damages were artificially introduced by a release of supports and insertion of cracks. Piombo et al. (2000) modeled the vehicle–bridge interaction system as a three-span orthotropic plate subject to a seven degrees-of-freedom multi-body system with linear suspensions and tires flexibility, and wavelet technique is used to extract the modal parameters. Lee et al. (2002) studied the identification of the operational

modal properties of a bridge structure using vibration data caused by the traffic loadings and the damage assessment based on the estimated modal parameters using the neural networks technique. Majumder and Manohar (2003) developed a time domain formulation to detect damages in a beam using data originating from the linear beam-oscillator dynamic interaction and extended the capabilities of this formulation to include the possibility of the damaged beam structure undergoing nonlinear vibrations. The study combines finite element modeling for the vehicle–bridge system with a time-domain formulation to detect changes in structural parameters. The structural properties and motion characteristics of the moving vehicle are assumed to be available, and the elemental stiffness loss is used to simulate the different damage scenarios.

In this paper, the operational deflection time history of the bridge subject to a moving vehicular load is analyzed using the continuous wavelet transform. A new technique is proposed for structural damage detection based on spatial wavelet analysis of response measurements at one point of the bridge deck. The mode shape of the beam with local damages is expressed as discrete unit step functions with stiffness of the local damages. The damage index based on wavelet coefficient is used as an indicator of the damage extent. In the simulation, the vehicle is modeled as a moving load, and the bridge is simplified as a continuous Euler–Bernoulli beam simply-supported at both ends. The effect of the parameters of the vehicle–bridge interaction system and noise in the measurements on the damage detection is studied. An experimental study is carried out on a reinforced concrete bridge model with a Tee-section subject to vehicle loadings to verify the method. Simulation and laboratory results show that the method is effective to detect crack damage in the concrete bridge structure under moving vehicular loads. Locations of multiple damages can be located accurately, and the results are not sensitive to measurement noise, speed and magnitude of moving load, measuring location, etc.

2. Dynamic behavior of cracked bridge beam subject to moving load

2.1. Equation of motion

The bridge–vehicle system is modeled as continuous beam subject to a moving load $P(t)$ as shown in Fig. 1. The load is assumed to be moving at a prescribed velocity $v(t)$, along the axial direction of the beam from left to right. The beam is assumed to be an Euler–Bernoulli beam. The equation of motion can be written as

$$\rho A \frac{\partial^2 w(x,t)}{\partial t^2} + C \frac{\partial w(x,t)}{\partial t} + \frac{\partial^2}{\partial x^2}\left(EI(x)\frac{\partial^2 w(x,t)}{\partial x^2}\right) = P(t)\delta(x - \hat{x}(t)) \tag{1}$$

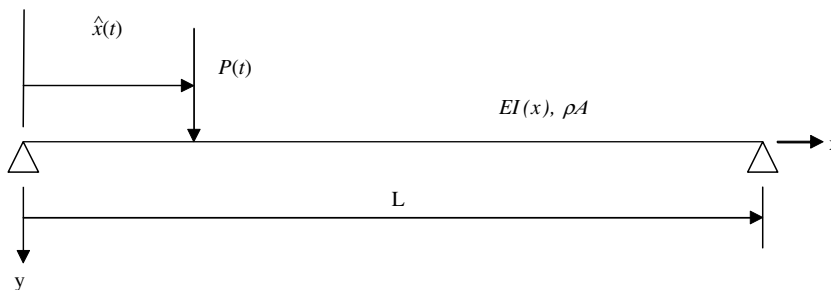Fig. 1. A continuous beam subject to moving loads.

where ρA, C are the mass per unit length and the damping of the beam, $EI(x)$ is flexural stiffness of the Euler–Bernoulli beam. $w(x,t)$ is the displacement function of the beam. $\hat{x}(t)$ is the location of moving load $P(t)$ at time t and $\delta(t)$ is the Dirac delta function. Express the transverse displacement $w(x,t)$ in modal coordinates

$$w(x,t) = \sum_{i=1}^{\infty} \phi_i(x)q_i(t) \tag{2}$$

where $\phi_i(x)$ is the mode shape function of the ith mode; $q_i(t)$ is the ith modal amplitude. Substituting Eq. (2) into Eq. (1), and multiplying by $\phi_i(x)$, integrating with respect to x between 0 and L, and applying the orthogonality conditions, we obtain

$$\frac{\mathrm{d}^2 q_i(t)}{\mathrm{d}t^2} + 2\xi_i\omega_i\frac{\mathrm{d}q_i(t)}{\mathrm{d}t} + \omega_i^2 q_i(t) = \frac{1}{M_i}P(t)\phi_i(\hat{x}(t)) \tag{3}$$

where ω_i, ξ_i, M_i are the modal frequency, damping ratio and the modal mass of the ith mode, and

$$M_i = \int_0^L \rho A\phi_i^2(x)\,\mathrm{d}x \tag{4}$$

The displacement of the beam at point x and time t can be found from Eqs. (2) and (3) as

$$w(x,t) = \sum_{i=1}^{\infty} \frac{\phi_i(x)}{M_i}\int_0^t h_i(t-\tau)P(\tau)\phi_i(\hat{x}(\tau))\,\mathrm{d}\tau \tag{5}$$

where

$$h_i(t) = \frac{1}{\omega_i'}\mathrm{e}^{-\xi_i\omega_i t}\sin\omega_i' t; \quad \omega_i' = \omega_i\sqrt{1-\xi_i^2} \tag{6}$$

2.2. Modal analysis of cracked beam structures

Fig. 2 shows a uniform bridge beam structure with N cracks. The damaged continuous beam is discretized into $N+1$ segments of constant unit weight ρA, bending stiffness EI (undamaged beam stiffness) and length l_i, $(i = 1, 2, \ldots, N+1)$. The segments are connected together through rotational springs (damage section) whose stiffness are denoted by k_i $(i = 1, 2, \ldots, N)$.
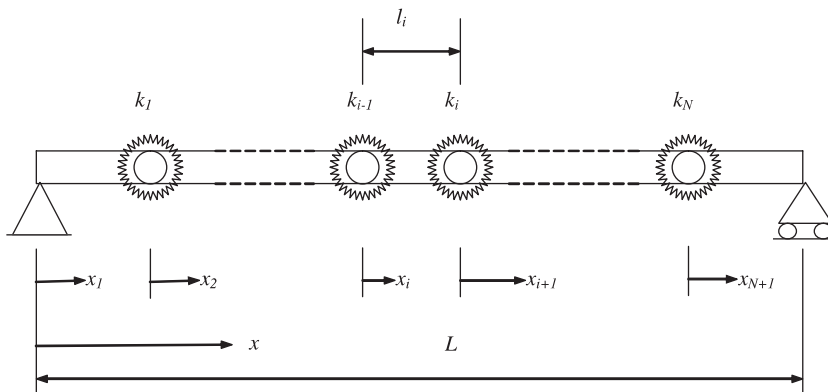

Fig. 2. Beam with rotational springs representing damaged section.

The eigen-function of an Euler–Bernoulli beam segment can be written as

$$r_i(x_i) = A_i \sin \beta x_i + B_i \cos \beta x_i + C_i \sinh \beta x_i + D_i \cosh \beta x_i, \quad (i = 1, 2, \ldots, N+1) \tag{7}$$

where $r_i(x_i)$ is the eigen-function for the ith segment, and β is the eigenvalue of the beam. Zhu and Law (2003) have presented the formulation of eigen-function for a multi-span continuous beam. We have a similar problem with $N+1$ segments connected by rotational springs here. The boundary conditions for the damaged beam are listed as follows:

$$r_1(x_1)|_{x_1=0} = r_{N+1}(x_{N+1})|_{x_{N+1}=l_{N+1}} = 0$$

$$\left. \frac{\partial^2 r_1(x_1)}{\partial x_1^2} \right|_{x_1=0} = \left. \frac{\partial^2 r_{N+1}(x_{N+1})}{\partial x_{N+1}^2} \right|_{x_{N+1}=l_{N+1}} = 0$$

$$\begin{cases} r_i(x_i)|_{x_i=l_i} = r_{i+1}(x_{i+1})|_{x_{i+1}=0} \\ \left. \dfrac{\partial r_i(x_i)}{\partial x_i} \right|_{x_i=l_i} + \dfrac{EI}{k_i} \left. \dfrac{\partial^2 r_i(x_i)}{\partial x_i^2} \right|_{x_i=l_i} = \left. \dfrac{\partial r_{i+1}(x_{i+1})}{\partial x_{i+1}} \right|_{x_{i+1}=0} \\ \left. \dfrac{\partial^2 r_i(x_i)}{\partial x_i^2} \right|_{x_i=l_i} = \left. \dfrac{\partial^2 r_{i+1}(x_{i+1})}{\partial x_{i+1}^2} \right|_{x_{i+1}=0} \qquad (i=1,2,\cdots,N) \\ \left. \dfrac{\partial^3 r_i(x_i)}{\partial x_i^3} \right|_{x_i=l_i} = \left. \dfrac{\partial^3 r_{i+1}(x_{i+1})}{\partial x_{i+1}^3} \right|_{x_{i+1}=0} \end{cases} \tag{8}$$

Substituting Eq. (7) into the boundary conditions (8), the mode shape of the continuous beam with N damage locations can be written as

$$\phi(x) = r_1(x)(1 - H(x - l_1)) + \sum_{i=2}^{N+1} r_i\left(x - \sum_{j=1}^{i-1} l_j\right)\left(H\left(x - \sum_{j=1}^{i-1} l_j\right) - H\left(x - \sum_{j=1}^{i} l_j\right)\right) \tag{9}$$

where $H(x)$ is the unit step function.

$$\begin{cases} r_1(x) = A_1 \sin \beta x + C_1 \sinh \beta x, & (0 \leqslant x < l_1) \\ r_i(x) = A_i(x) \sin \beta x + B_i \cos \beta x + C_i \sinh \beta x + D_i \cosh \beta x, & (0 \leqslant x < l_i,\ i = 2, 3, \ldots, N+1) \end{cases} \tag{10}$$

where parameters $\{A\} = \{\beta, A_1, C_1, A_i, B_i, C_i, D_i\ (i = 2, 3, \ldots, N+1)\}$ are determined from the following equation

$$[\mathbf{S}]\{\mathbf{A}\} = \mathbf{0} \tag{11}$$

where the elements of matrix S are given by

$$f_{11} = \sin \beta l_1, \quad f_{12} = \sinh \beta l_1, \quad f_{14} = -1, \quad f_{16} = -1$$

$$f_{21} = -\sin \beta l_1, \quad f_{22} = \sinh \beta l_1, \quad f_{24} = 1, \quad f_{26} = -1$$

$$f_{31} = -\cos \beta l_1, \quad f_{32} = \cosh \beta l_1, \quad f_{33} = 1, \quad f_{35} = -1$$

$$f_{41} = \beta \cos \beta l_1 - \beta^2 \frac{EI}{k_1} \sin \beta l_I, \quad f_{42} = \beta \cosh \beta l_1 + \beta^2 \frac{EI}{k_1} \sinh \beta l_1, \quad f_{43} = -\beta, \quad f_{45} = -\beta$$

$$f_{4(i-1)+1,4(i-1)-1} = \sin \beta l_i, \quad f_{4(i-1)+1,4(i-1)} = \cos \beta l_i$$

$$f_{4(i-1)+1,4(i-1)+1} = \sinh \beta l_i, \quad f_{4(i-1)+1,4(i-1)+2} = \cosh \beta l_i$$

$$f_{4(i-1)+1,4(i-1)+4} = -1, \quad f_{4(i-1)+1,4(i-1)+6} = -1,$$

$$f_{4(i-1)+2,4(i-1)-1} = -\sin\beta l_i, \quad f_{4(i-1)+2,4(i-1)} = -\cos\beta l_i$$

$$f_{4(i-1)+2,4(i-1)+1} = \sinh\beta l_i, \quad f_{4(i-1)+2,4(i-1)+2} = \cosh\beta l_i$$

$$f_{4(i-1)+2,4(i-1)+4} = 1, \quad f_{4(i-1)+2,4(i-1)+6} = -1,$$

$$f_{4(i-1)+3,4(i-1)-1} = -\cos\beta l_i, \quad f_{4(i-1)+3,4(i-1)} = \sin\beta l_i$$

$$f_{4(i-1)+3,4(i-1)+1} = \cosh\beta l_i, \quad f_{4(i-1)+3,4(i-1)+2} = \sinh\beta l_i$$

$$f_{4(i-1)+3,4(i-1)+3} = 1, \quad f_{4(i-1)+3,4(i-1)+5} = -1,$$

$$f_{4(i-1)+4,4(i-1)-1} = \beta\cos\beta l_i - \beta^2\frac{EI}{k_i}\sin\beta l_i, \quad f_{4(i-1)+4,4(i-1)} = -\beta\sin\beta l_i - \beta^2\frac{EI}{k_i}\cos\beta l_i$$

$$f_{4(i-1)+4,4(i-1)+1} = \beta\cosh\beta l_i + \beta^2\frac{EI}{k_i}\sinh\beta l_i, \quad f_{4(i-1)+4,4(i-1)+2} = \beta\sinh\beta l_i + \beta^2\frac{EI}{k_i}\cosh\beta l_i$$

$$f_{4(i-1)+4,4(i-1)+3} = -\beta, \quad f_{4(i-1)+4,4(i-1)+5} = -\beta,$$

$$f_{4N+1,4N-1} = \sin\beta l_{N+1}, \quad f_{4N+1,4N} = \cos\beta l_{N+1}, \quad f_{4N+1,4N+1} = \sinh\beta l_{N+1}$$

$$f_{4N+1,4N+2} = \cosh\beta l_{N+1}, \quad f_{4N+2,4N-1} = -\sin\beta l_{N+1}, \quad f_{4N+2,4N} = -\cos\beta l_{N+1}$$

$$f_{4N+2,4N+1} = \sinh\beta l_{N+1}, \quad f_{4N+2,4N+2} = \cosh\beta l_{N+1}, \quad (i = 2, 3, \ldots, N)$$

3. Crack identification using continuous wavelet transform

Eq. (9) shows that there are discontinuities at the damage points, especially the slope discontinuities at the cracks. The damaged locations can be determined by finding the discontinuous points in the mode shapes. Mode shape curvature is widely used to find these discontinuous points (Pandey et al., 1991). However, the first problem for damage detection using curvature directly is to calculate the curvature by derivation. It is very difficult to obtain accurate mode shape in practice and the differentiation of the mode shape will further amplify the measurement error. Recently, the wavelet transform is widely used to measure the local regularity of a signal.

3.1. The continuous wavelet transform of measured displacement

The continuous wavelet transform of a square-integrable signal $f(x)$, where x is time or space, is defined as (Mallat and Hwang, 1992)

$$Wf(u,s) = f(x) \otimes \psi_s(x) = \frac{1}{\sqrt{s}} \int_{-\infty}^{+\infty} f(x)\psi^*\left(\frac{x-u}{s}\right) dx \tag{12}$$

where $\otimes$ denotes the convolution of two functions. $\psi_s(x)$ is the dilation of $\psi(x)$ by the scale factor s. u is the translation indicating the locality. $\psi^*(x)$ is the complex conjugate of $\psi(x)$ which is a mother wavelet satisfying the following admissibility condition:

$$\int_{-\infty}^{+\infty} \frac{|\Psi(\omega)|^2}{|\omega|} d\omega < +\infty \tag{13}$$

where $\Psi(\omega)$ is the Fourier transform of $\psi(x)$. The existence of the integral in (13) requires that

$$\Psi(0) = 0 \text{ i.e., } \int_{-\infty}^{+\infty} \psi(x) dx = 0 \tag{14}$$

From Eq. (5),the displacement at x_m can be written as

$$w(x_m, t) = \sum_{i=1}^{\infty} \frac{\phi_i(x_m)}{M_i} \int_0^t h_i(t - \tau) P(\tau) \phi_i(\hat{x}(\tau)) \, \mathrm{d}\tau \tag{15}$$

The second derivation of the displacement with respect to the position of the moving load can be obtained as

$$\frac{\partial^2 w(x_m, t)}{\partial^2 \hat{x}_l(t)} = \sum_{i=1}^{\infty} \frac{\phi_i(x_m)}{M_i} \int_0^t h_i(t - \tau) P(\tau) \frac{\partial^2 \phi_i(\hat{x}(\tau))}{\partial \hat{x}(\tau)^2} \, \mathrm{d}\tau \tag{16}$$

where $\frac{\partial^2 \phi_i(x)}{\partial x^2}$ is the second order derivation of the ith mode which is the curvature of the displacement mode shape. This shows that the second derivative of the displacement with respect to the load position includes the curvature information of the mode.

3.2. The multiscale differential operator of wavelet (Mallat and Hwang, 1992)

Let us take the Gaussian function $\theta(x)$ the wavelet of which can be defined as the second derivative of the function:

$$\psi(x) = \frac{\mathrm{d}^2 \theta(x)}{\mathrm{d}x^2} \tag{17}$$

The wavelet $\psi(x)$ in Eq. (17) is continuous differentiable and is usually referred to as the Mexican Hat wavelet that has the following explicit expression:

$$\psi(x) = \frac{2}{\sqrt{3}\sigma} \pi^{-1/4} \left(\frac{x^2}{\sigma^2} - 1 \right) \exp\left(\frac{-x^2}{2\sigma^2} \right) \tag{18}$$

where σ is the standard deviation.

The wavelet transform for the displacement $w(xm, t)$ is then expressed by the following relation (Mallat and Hwang, 1992) when the Mexican Hat wavelet is adopted, as

$$Ww(\hat{x}(t), s) = w(x_m, t) \otimes \psi_s(\hat{x}(t)) = s^2 \frac{\mathrm{d}^2}{\mathrm{d}\hat{x}(t)^2} (w(x_m, t) \otimes \theta_s)(\hat{x}(t)) \tag{19}$$

Eq. (19) is the multi-scale differential operator of the second order, and is the relation between the second differentiability of $w(x_m, t)$ and its wavelet transform decay at fine scales. The wavelet transform $Ww(\hat{x}(t), s)$ is proportional to the second derivative of $w(x_m, t)$ smoothed by the Gaussian function $\theta_s(x)$. So the wavelet transform can be used to replace the direct differentiation of the displacement to get the curvature properties. The second differential of operating curvature shapes of a beam is not continuously differentiable at the damage location, while in the present case the measured location is continuously differentiable. The damage can then be located using the wavelet transform of the operational displacement time history at one point when the beam structure is subject to the action of the moving load. Similar formulation can be obtained for accelerations.

4. Numerical studies

Table 1 shows the frequency ratios between the cracked and uncracked states of a simply supported beam with an open crack at mid-span with different crack depth ratios, δ, calculated from Eq. (11) and from

Table 1
Frequency ratio between cracked to uncracked simply supported beam (length/height ratio = 36.22)

Mode	Crack depth ratio δ											
	1/4		1/3		2/5		1/2		3/5		2/3	
	Present	[17]	Present	[17]	Present	[17]	Present	[17]	Present	[17]	Present	[17]
First	0.986	0.984	0.972	0.970	0.954	0.953	0.909	0.903	0.835	0.824	0.767	0.755
Third	0.986	0.984	0.973	0.972	0.957	0.957	0.922	0.917	0.872	0.866	0.836	0.830

Narkis (1994). The beam length to beam height ratio is 36.22. The first and third natural frequency ratios calculated from Eq. (11) are very close to the results by Narkis (1994).

4.1. Example 1: A simply supported beam with a single crack

A simply supported beam of 50 m length, 1.0 m high and 0.5 m width (Mahmoud, 2001) is used. The Young's modulus and density of the beam are $E = 2.1 \times 10^{11}$ Pa and $\rho = 7860$ kg/m^3, and the moving load is $F_0 = 10$ kN. The first six natural frequencies are 0.94, 3.75, 8.44, 15.00, 23.44, 33.75 Hz. According to Tada et al. (2000), the crack compliance C_C of a rectangular beam with the crack depth ratio δ is as follow:

$$C_C = \frac{1}{k} = \frac{2h}{EI}\left(\frac{\delta}{1-\delta}\right)^2 [5.93 - 16.69\delta + 37.14\delta^2 - 35.84\delta^3 + 13.12\delta^4] \tag{20}$$

Fig. 3 shows the normalized deflection versus the position of the moving load at mid-span for the undamaged beam and for a cracked beam (crack at mid-span with the crack depth ratio $\delta = 0.5$) for different load speeds. The normalized deflection is relative to the value $F_0 L^3/(48EI)$, which is the static
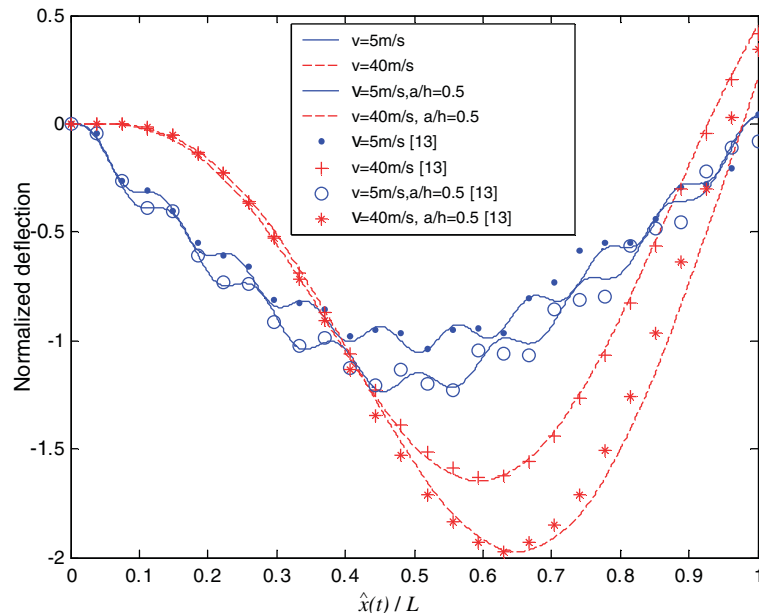

Fig. 3. Normalized deflection at mid-span by Mahmoud (2001) and the present method.

deflection due to the load at mid-span. The sampling rate is 100 Hz. The results by the present algorithm are close to those in the reference (Mahmoud, 2001). It shows that the algorithm in the paper has similar accuracy as the existing method.

4.2. Damage location identification

The above simply-supported beam is used in the simulation and the damping ratio for all modes is taken equal to 0.02. The crack is at $1/3L$ with a depth ratio of 0.5. White noise is added to the calculated responses of the beam to simulate the polluted measurements, and 1%, 3% and 5% noise levels are studied separately.

$$w = w_{calculated} + E_p N_{oise} \sigma(w_{calculated}) \tag{21}$$

where w is the polluted displacement. E_p is the noise level and N_{oise} is a standard normal distribution vector with zero mean value and unit standard deviation. $w_{calculated}$ is the calculated displacement, and $\sigma(w_{calculated})$ is their standard deviations. Continuous wavelet transform on the displacement time history at mid-span is calculated with dilation s equals 1 to 512 in unit increment.

Fig. 4 shows the wavelet coefficients of the displacement at mid-span with scale 64 when the moving load is on top of the beam. Fig. 5 shows the location of the peak from using different scales. Fig. 6 shows the logarithm value of the minimum wavelet coefficients obtained from using different scales. The following observations are made.

(1) Fig. 4 shows that there is a dip in the curve of wavelet coefficients at $1/3L$ which is the location of the damage. In other words, the damage location can be determined as the location of the dip in the wavelet coefficient curve.
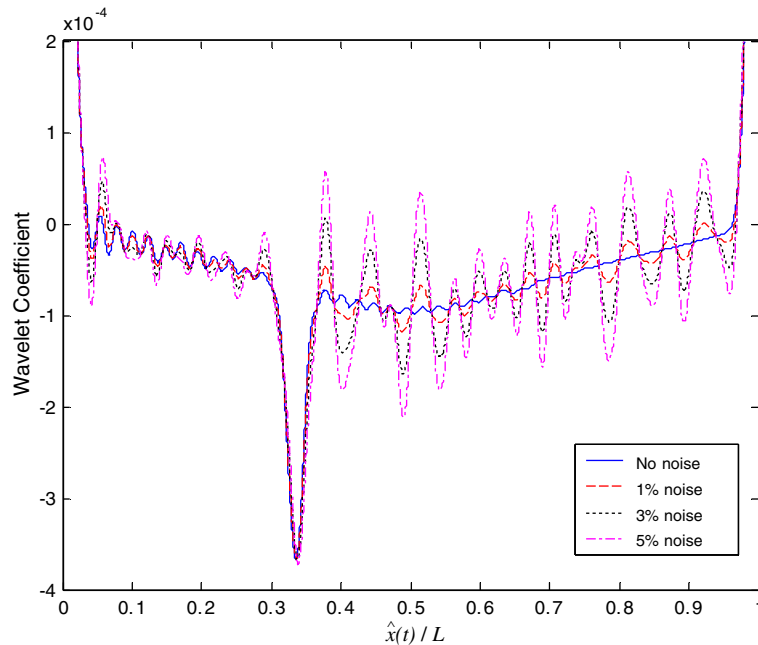

Fig. 4. Wavelet coefficients of the displacement at mid-span when a moving load is moving on the beam at 1 m/s.
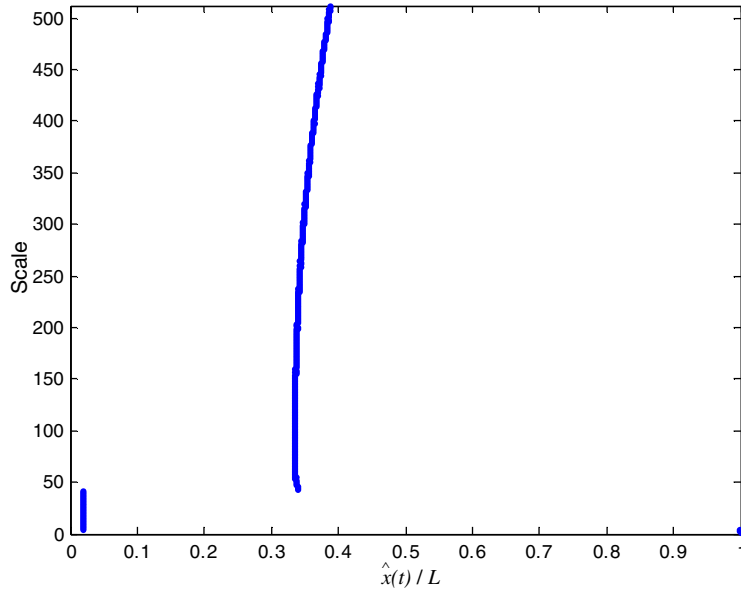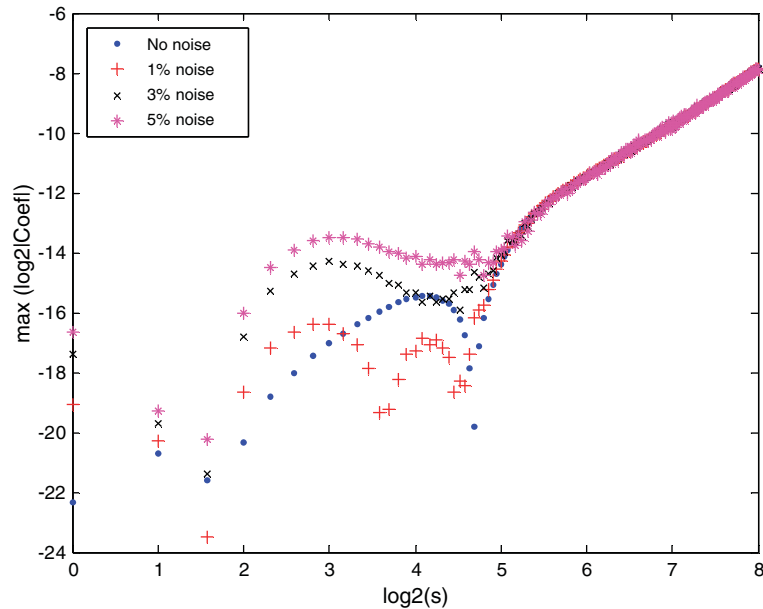
Fig. 5. The dip peak position versus scale plot.

Fig. 6. Wavelet coefficients of the response with different noise levels.

(2) In Fig. 5, the position of the dip in the wavelet coefficient curve is close to $1/3L$ when the scale is not less than 42 and they are close to the two ends when the scale is less than 42. The latter is associated with the discontinuity of the measured responses on the entry and exit of the moving load. When the scale is larger than 42, the position of the dip indicates the position of the damage.

(3) The dip value of wavelet coefficient is plotted versus the scale in a log-log plot in Fig. 6 when different noise level is included in the response. The results are close to each other when the scale is larger than 28. This means the identified location of damage is least affected by measurement noise when the scale is larger than 28.

4.3. Damage extend estimation

The parameters are the same as for the above studies. Based on observations in the last study, scale 64 is adopted in this study. Fig. 7 shows the wavelet coefficients of the response at mid-span with different crack depths when the moving load is moving on the beam. The dip value in the curves becomes smaller when the crack depth increases, but the position of the dip does not change. A damage index is defined to express the damage extent as follow

$$\alpha = \frac{\log_2|Wf(u_{\mathrm{d}}, s)|}{\log_2|Wf_{\mathrm{o}}(u_{\mathrm{d}}, s)|} \tag{22}$$

where u_{d} is the damage location and $Wf_{\mathrm{o}}(u_{\mathrm{d}}, s)$ is the wavelet coefficient of the response without damage at location u_{d}.

Table 2 shows the damage indices defined by Eq. (22) for cracks at different location from different measurement of noisy data. The damage index reduces when the crack depth increases, and the measuring noise has little effect on the value of the damage index. The corresponding relationship between the damage index and the crack depth can be determined for a beam as a database for assessment of a particular crack damage in future measurements.
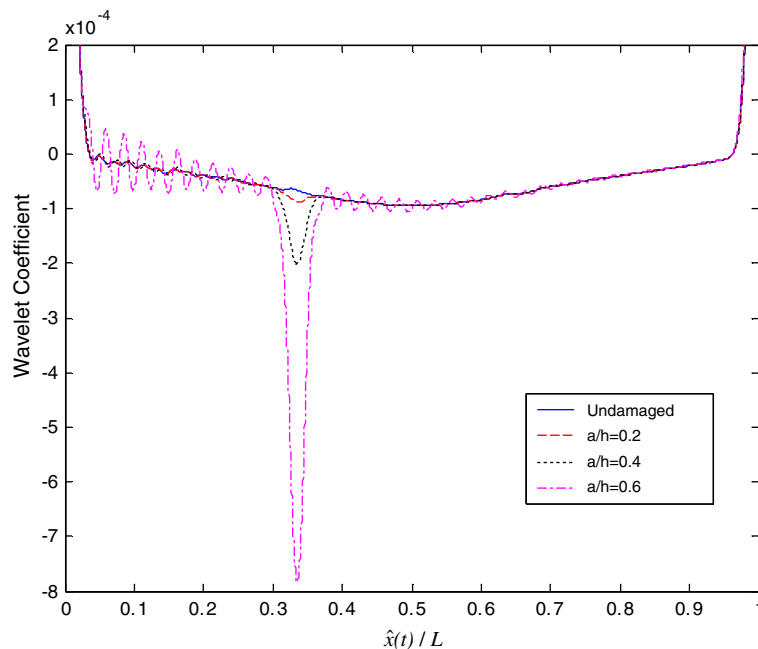

Fig. 7. Wavelet coefficients with various crack depth and 3% noise in the response.

Table 2
Damage indices of the cracked beam

Measuring Location	δ	0.1	0.2	0.3	0.4	0.5	0.6	0.7	0.8	0.9
1/3L	No noise	0.992	0.971	0.935	0.884	0.822	0.743	0.646	0.561	0.410
	1%	0.992	0.700	0.933	0.881	0.819	0.740	0.643	0.559	0.408
	3%	0.991	0.967	0.928	0.874	0.811	0.732	0.636	0.553	0.404
	5%	0.990	0.964	0.923	0.867	0.803	0.724	0.629	0.546	0.400
1/2L	No noise	0.992	0.969	0.932	0.880	0.810	0.732	0.632	0.538	0.378
	1%	0.992	0.970	0.933	0.882	0.815	0.734	0.634	0.539	0.379
	3%	0.993	0.971	0.936	0.886	0.819	0.737	0.638	0.542	0.380
	5%	0.993	0.972	0.938	0.888	0.822	0.741	0.641	0.545	0.382
2/3L	No noise	0.992	0.971	0.937	0.888	0.825	0.749	0.656	0.543	0.505
	1%	0.991	0.968	0.930	0.879	0.815	0.738	0.647	0.535	0.499
	3%	0.988	0.956	0.911	0.854	0.788	0.711	0.621	0.516	0.483
	5%	0.977	0.927	0.869	0.806	0.738	0.664	0.579	0.479	0.454

4.4. Parametric study

Fig. 8 shows the wavelet coefficients of the response at mid-span with 3% noise when the load is moving on the beam at different speeds. The crack location is at 1/3L and the crack depth ratio is 0.5. Other parameters are the same as for the last study. Fig. 9 shows the wavelet coefficients of the responses at 1/4L, 1/2L and 3/4L, respectively. Fig. 10 shows the results when loads of different magnitude are moving on the beam. From these results, the following observations are made.
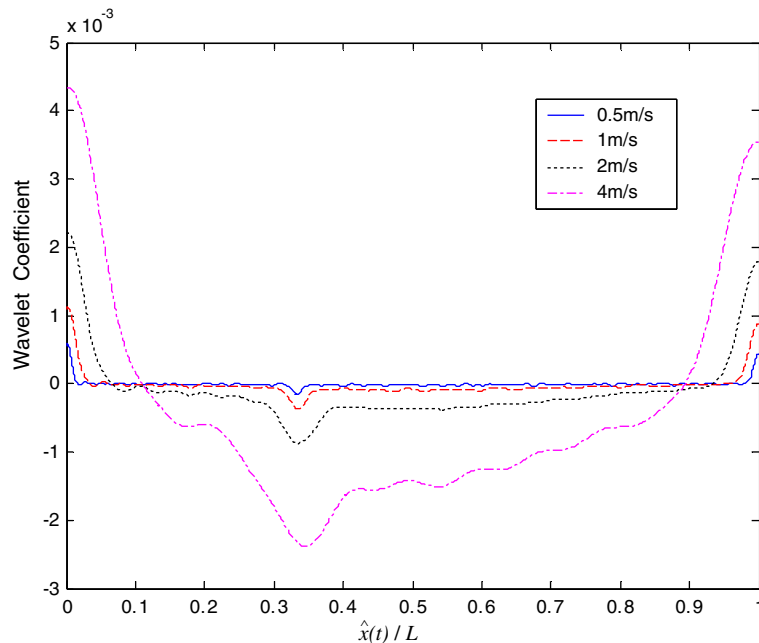

Fig. 8. Wavelet coefficients with the load moving at different speeds (3% noise).
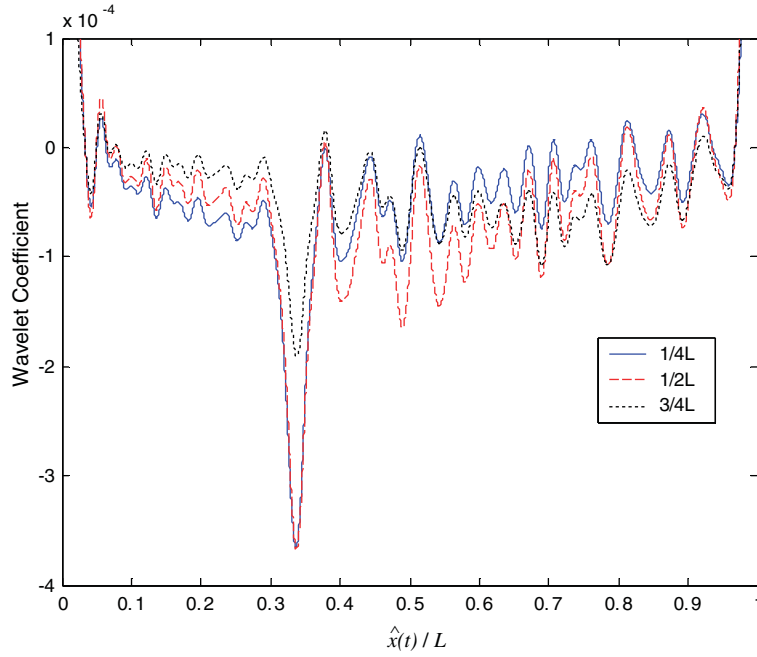
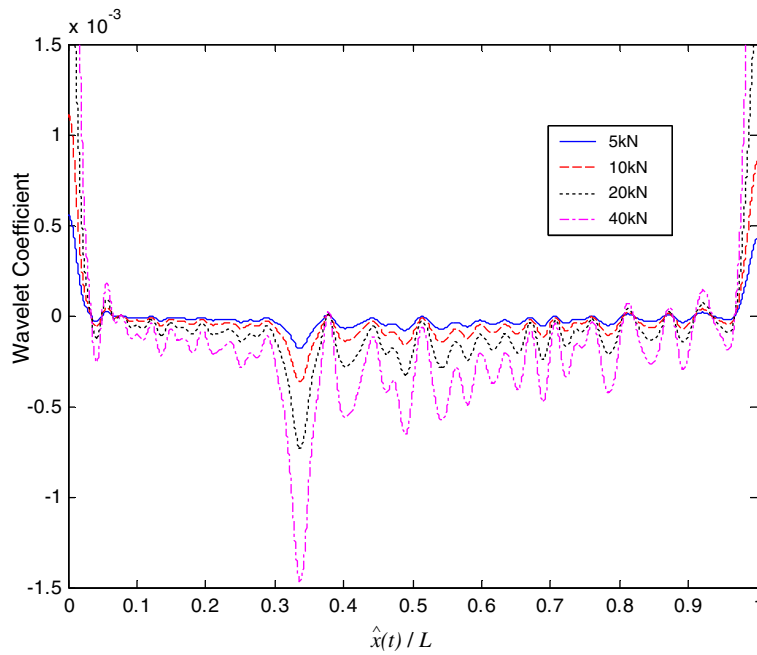Fig. 9. Wavelet coefficients of the response at different measuring locations.

Fig. 10. Wavelet coefficients of the response at mid-span when different moving loads are moving on the beam.

1) Fig. 8 shows that the moving speed of the load has a significant effect on the value of the wavelet coefficient, but the position of the dip does not change with the moving speed.
2) The position of the dip remains close to the damage location when the responses obtained from different measuring locations are used in the calculation. The value of the dip in the wavelet coefficient curves is different for different measuring locations as shown in Fig. 9. The absolute value from using response at $1/4L$ or $1/2L$ is larger than that at $3/4L$. This is because the former group of measuring location is closer to the damage location at $1/3L$ than the latter.
3) As shown in Fig. 10, the position of the dip in the wavelet coefficient curve remains close to the damage location when different loads are moving on the beam, and the value of the dip decreases with an increase in the moving load.

4.5. Example 2: A simply supported beam with multiple cracks

A simply supported beam with multiple cracks subject to a moving load is studied in this section. The parameters of the beam and the moving load are the same as for the above studies except for the multiple damages in the beam. The crack depth ratios of all cracks is 0.5, and 3% noise is included in the simulation. Fig. 11 shows the wavelet coefficients of the responses at $1/4L, 1/2L$ and $3/4L$ with four cracks located at $1/5L, 2/5L, 3/5L$ and $4/5L$. Fig. 12 gives the results for the beams with two cracks at different spacing. The crack depth ratios are also 0.5. The following observations are noted.

1) There are four dips in the wavelet coefficient curves in Fig. 11. The dip positions are close to the damage locations at $1/5L, 2/5L, 3/5L$ and $4/5L$, and the dip value varies with the measuring location. The multiple damage locations can be determined accurately from the wavelet coefficient of the response obtained from a single measuring point.
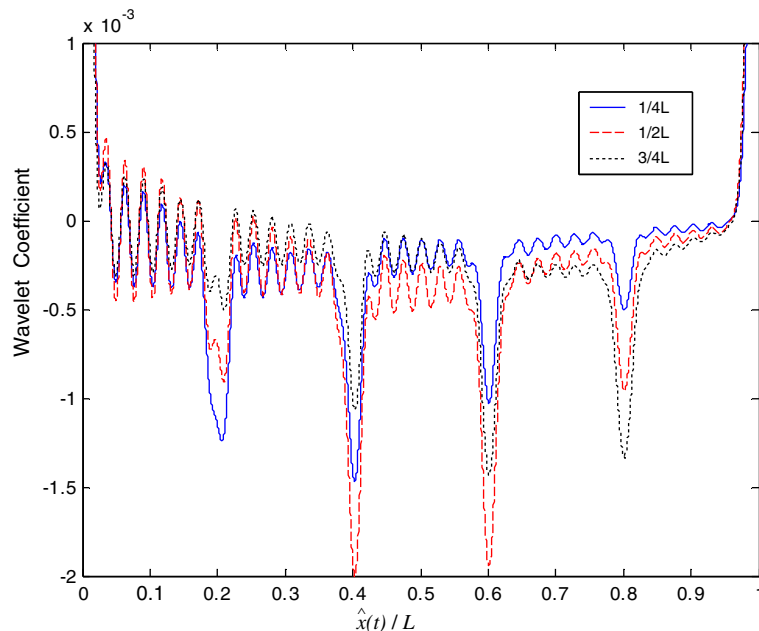

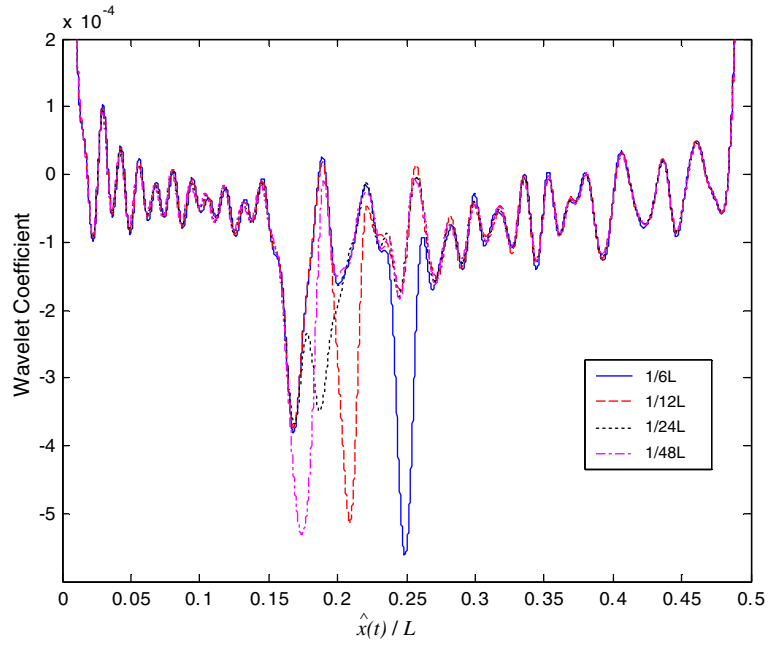Fig. 11. Wavelet coefficients of the responses with four damages (3% noise).

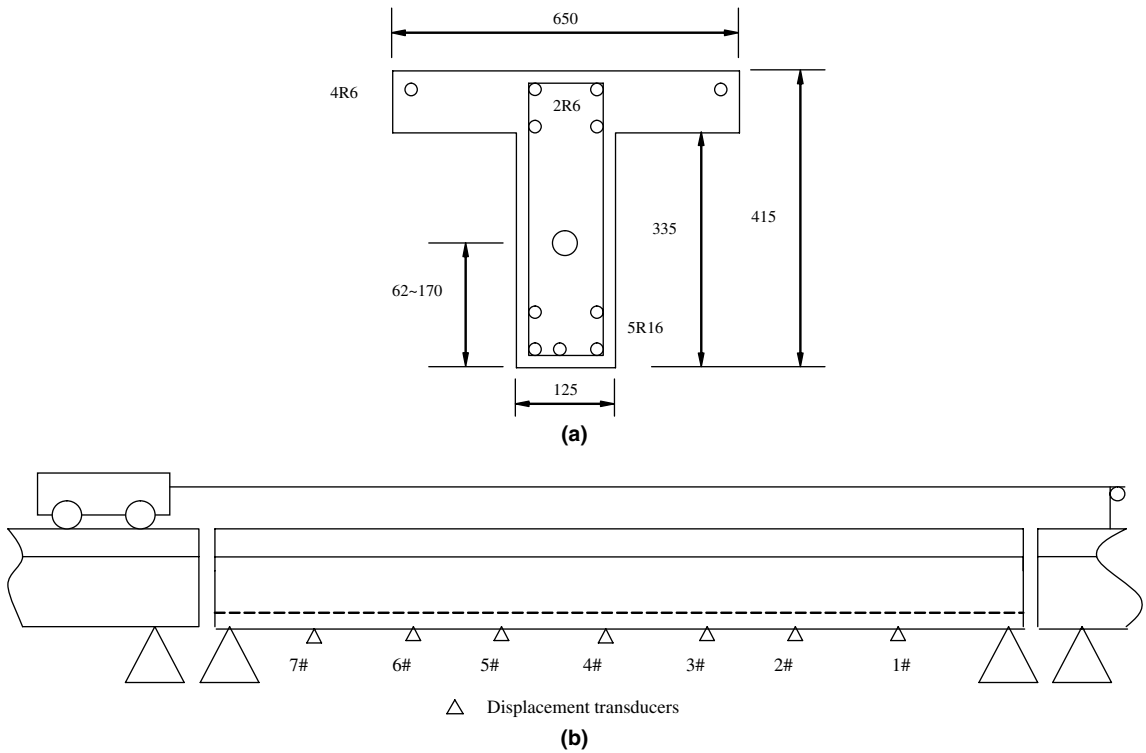Fig. 12. Wavelet coefficients of the response at mid-span with various spacing between two cracks.

Fig. 13. (a) Cross-section layout of the reinforced concrete beam. (b) Experimental setup.

2) Fig. 12 shows that there are two dips in the curve of wavelet coefficient when the distance between two cracks is not smaller than 1/24L, and there is only one dip when the distance is 1/48L. This shows that the damages can be separated identified clearly when the spacing is not smaller than 1/24L.

5. Experimental investigation

The experimental setup shown in Fig. 13 includes three Tee-section concrete beams, i.e. the leading beam, the main beam and the tailing beam. The length of the leading and tailing beams are 4.5 m each, and the main beam is 5.0 m long. The gaps between the beams are 10 mm. A vehicle was pull along the beam by an electric motor at an approximate speed of 0.5 m/s. The axle spacing of the vehicle was 0.8 m, and the wheel spacing was 0.39 m. The vehicle weighed 10.60 kN, with the front axle load weighed 5.58 kN and the rear axle load weighed 5.02 kN. As the total mass of the concrete beam was 1050 kg, the weight ratio between the vehicle and bridge was 1.01.

Seven displacement transducers (sensors 1# to 7#) were evenly distributed at the bottom and along the beam to measure the responses as marked in Fig. 13. Thirteen photo-electric sensors were installed on the leading beam and the main beam at 0.56 m spacing to monitor the speed of the vehicle. The third and thirteenth photo-electric sensors were located at the entry and exit points of the main beam separately. INV300E data acquisition system was used to collect the data from all the eight channels. The sampling frequency was 2024.292 Hz, and the sampling period was 30 s for each test.
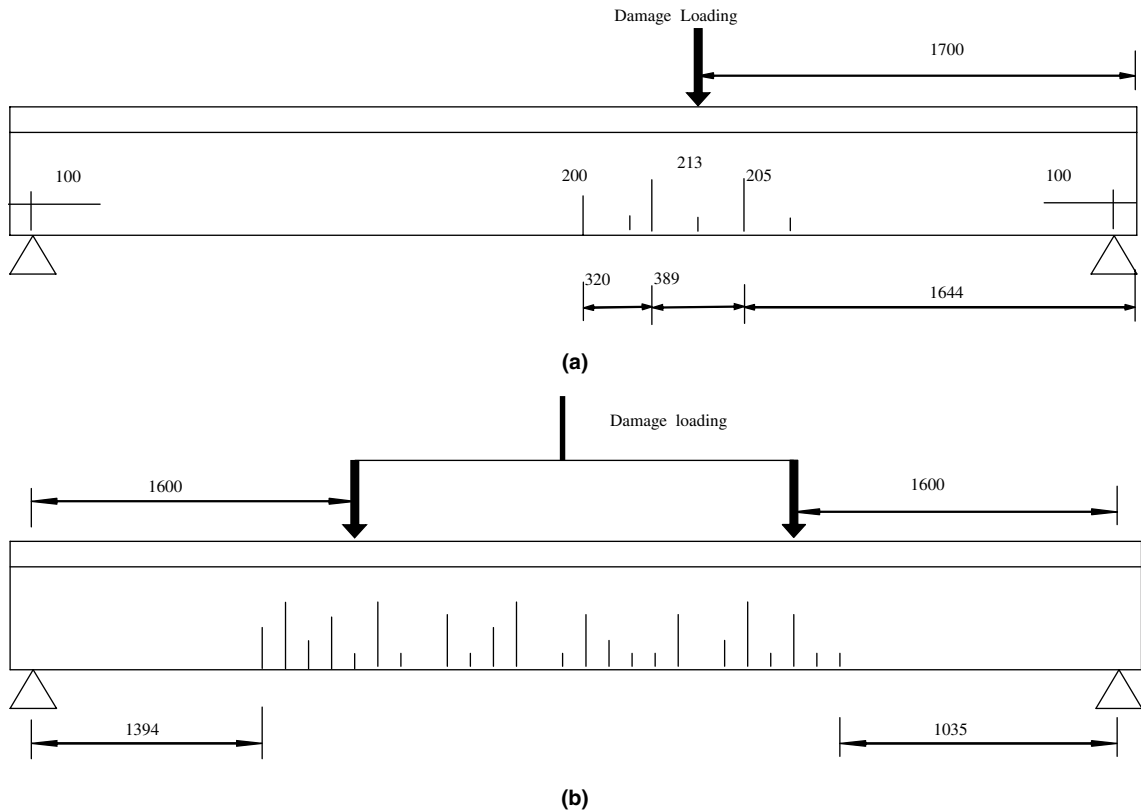

Fig. 14. Damage loading and the crack zone. (a) First step and (b) second step.

Damage in the beam was created using a three-point load system applied at 1/3L from the right support of the beam as shown in Fig. 14 (a). The load was gradually increased at 2 kN increment. When 36 kN was reached, several tensile cracks were clearly seen on the beam rib. When the load increased to 50 kN, the crack width of the largest crack at the bottom of the beam was measured as 0.10 mm. The location of this crack was close to the loading position but on the inside of the span with a visual crack depth of 213 mm and a crack zone of 760 mm wide. After the load was kept on the beam for 30 min, the beam was unloaded and the crack closed partly with the crack width at the bottom of the beam reduced to 0.025 mm. These observations are referred to as the small damage case.

For the large damage case, the beam was first loaded at 2/3L of the beam from the right support up to 50 kN using the three-point load system. This created a crack pattern similar in magnitude and extent to the existing crack zone at 1/3L. Further loading was made using a four-point load system as shown in Fig. 14(b). The final total load was 105 kN without yielding of the main reinforcement. The largest crack was close to the middle of the beam with 281 mm depth. The width of this crack at the bottom of the beam was 0.1 mm at 105 kN load, and it become 0.038 mm when the beam was unloaded after keeping the 105 kN static load on top for 30 min. The crack zone was measured 2371 mm long.

Fig. 15 shows the wavelet coefficients of the displacement at 3/8L (3# transducer) when the model car was moving on the concrete beam. There are mainly six peaks for the small damage case. The first and second peaks are associated with impacts on the entry of the front and rear axles. The fifth and sixth peaks are associated with impacts on the exit of the front and rear axles. The third and fourth peaks are related to the locations of the damage in Fig. 15(a). The results show that the damage location can be determined using the peaks in the wavelet coefficient of the response from a single measuring point. For the large damage case, there are many cracks created in the reinforced concrete beam. There are also many peaks in the curve
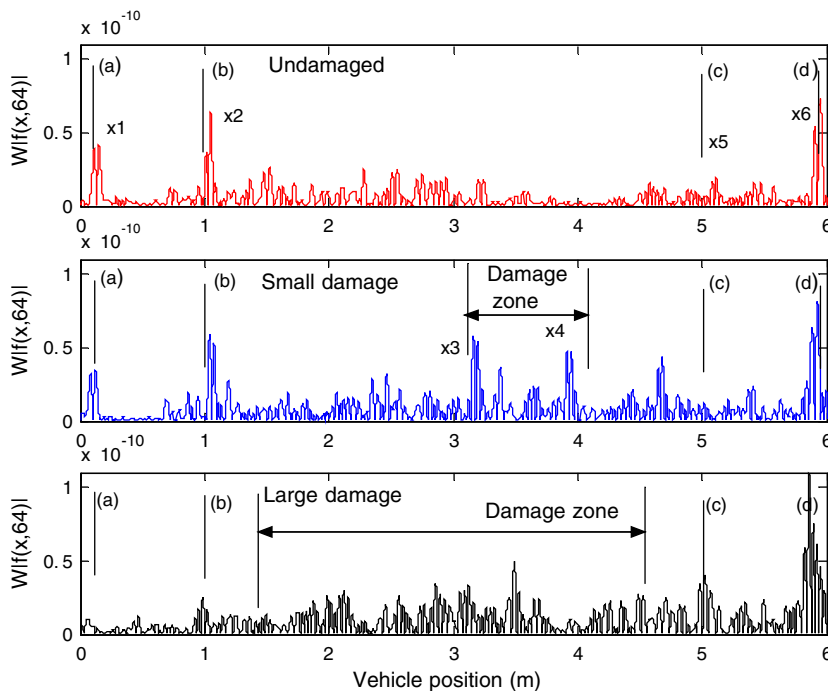

Fig. 15. Spatial wavelet coefficient at scale 64. (a) Denotes entry of first axle, (b) denotes entry of second axle, (c) denotes exit of first axle and (d) denotes exit of second axle.

of the wavelet coefficient besides those associated with the entry and exit of vehicle, and the damage zone can be clearly estimated, but the crack location can not be determined separately. This can be explained by the fact that the large static load of 105 kN has caused bond slippage between the steel bar and concrete, and the damage can not be simply modelled as an open crack.

6. Conclusions

A new technique for structural damage detection based on spatial wavelet analysis of the operational deflection time history obtained from a single measuring point of the bridge deck is proposed. Numerical simulation and experimental results show that the method is effective and the damage location can be determined accurately. The method can determine the damage location accurately even though there are multiple damages in the bridge beam. The location is determined as the position of the dip in the wavelet coefficient curve and there is no baseline requirement in determining the damage location. The damage extent can be determined using a reference database of the damage index based on the wavelet coefficient. The identified position associated with local damage in the beam does not vary with the measurement noise, the speed of the moving load, measuring location and the amplitude of the moving load. The method is robust in determining the damage location.

Acknowledgement

References

Abdel Wahab, M., De Roeck, G., 1997. Effect of temperature on dynamic system parameters of a highway bridge. Structural Engineering International 4, 266–270.

Chance, J., Thomlinson, G.R., Worden, K., 1994. A simplified approach to the numerical and experimental modeling of the synamics of a cracked beam. In: The 12th International Modal Analysis Conference, Honolulu, USA, pp. 778–785.

Chang, C.C., Chen, L.W., 2003. Vibration damage detection of a Timoshenko beam by spatial wavelet based approach. Applied Acoustics 64, 1217–1240.

Doebling, S.W., Farrar, C.R., Prime, M.B., 1998. A summary review of vibration-based damage identification methods. The Shock and Vibration Digest 30 (2), 91–105.

Douka, E., Loutridis, S., Trochidis, A., 2003. Crack identification in beams using wavelet analysis. International Journal of Solids and Structures 40, 3557–3569.

Farrar, C.R., Jauregui, D.A., 1998. Comparative study of damage identification algorithms applied to a bridge: I. Experiment. Smart Materials and Structures 7, 704–719.

Gentile, A., Messina, A., 2003. On the continuous wavelet transforms applied to discrete vibrational data for detecting open cracks in damaged beams. International Journal of Solids and Structures 40, 295–315.

Hoerst, B.C., Ratcliffe, C.P., 1997. Damage detection in beams using Laplacian operators on experimental modal data. In: The 15th International Modal Analysis Conference, Orlando, USA, pp. 1305–1311.

Hong, J.C., Kim, Y.Y., Lee, H.C., Lee, Y.W., 2002. Damage detection using the Lipschitz exponent estimated by the wavelet transform: applications to vibration modes of a beam. International Journal of Solids and Structures 39, 1803–1816.

Kijewski, T., Kareem, A., 2003. Wavelet transform for system identification in civil engineering. Computer-Aided Civil and Infrastructure Engineering 18 (5), 339–355.

Lee, J.W., Kim, J.D., Yun, C.B., Yi, J.H., Shim, J.M., 2002. Health-monitoring method for bridges under ordinary traffic loadings. Journal of Sound and Vibration 257 (2), 247–264.

Liew, K.M., Wang, Q., 1998. Application of wavelet theory for crack identification in structures. Journal of Engineering Mechanics ASCE 142 (2), 152–157.

Mahmoud, M.A., 2001. Effect of cracks on the dynamic response of a simple beam subject to a moving load. Proceedings of the Institute of Mechanical Engineers. Part F: Journal of Rail and Rapid Transit 215 (3), 207–215.

Majumder, L., Manohar, C.S., 2003. A time-domain approach for damage detection in beam structures using vibration data with a moving oscillator as an excitation source. Journal of Sound and Vibration 268 (4), 699–716.

Mallat, S., Hwang, W.L., 1992. Singularity detection and processing with wavelets. IEEE Transactions on Information Theory 38 (2), 617–643.

Mazurek, D.F., Dewolf, J.T., 1990. Experimental study of bridge monitoring techniques. Journal of Structural Engineering ASCE 115 (9), 2532–2549.

Narkis, Y., 1994. Identification of crack location in vibration simply supported beams. Journal of Sound and Vibration 172 (4), 549–558.

Pai, P.F., Young, L.G., 2001. Damage detection of beams using operational deflection shapes. International Journal of Solids and Structures 38, 3161–3192.

Pandey, A.K., Biswas, M., Samman, M.M., 1991. Damage detection from changes in curvature mode shapes. Journal of Sound and Vibration 145 (2), 321–332.

Piombo, B.A.D., Fasana, A., Marchesiello, S., Ruzzene, M., 2000. Modelling and identification of the dynamic response of a supported bridge. Mechanical Systems and Signal Processing 14 (1), 75–89.

Ratcliffe, C.P., Bagaria, W.J., 1998. Vibration technique for locating delamination in a composite beam. America Institute of Aeronautics and Astronautics Journal 36 (6), 1074–1077.

Salawu, O.S., 1997. Detection of structural damage through changes in frequency: a review. Engineering Structures 19 (9), 718–723.

Staszewski, W.J., 1998. Structural and mechanical damage detection using wavelets. The Shock and Vibration Digest 30 (6), 457–472.

Tada, H., Paris, P.C., Irwin, G.R., 2000. The Stress Analysis of Cracks Handbook. ASME Press, New York.

Wang, Q., Deng, X.M., 1999. Damage detection with spatial wavelets. International Journal of Solids and Structures 36, 3443–3468.

Zhu, X.Q., Law, S.S., 2003. Identification of moving interaction forces with incomplete velocity information. Mechanical Systems and Signal Processing 17 (6), 1349–1366.